Geothermics 124 (2024) 103133

Contents lists available at ScienceDirect

Geothermics

journal homepage: www.elsevier.com/locate/geothermics

Applicability of Na/K geothermometer to the metapelitic non-volcanic geothermal fields in the Taiwan orogenic belt

Yi-Chia Lu [a,b,c,*], Sheng-Rong Song [d], Ting-Jui Song [e], Chyi Wang [d], Andrew Tien-Shun Lin [b,a,c], Sachihiro Taguchi [f]

[a] *Graduate Institute of Applied Geology, National Central University, Taoyuan, Taiwan*
[b] *Department of Earth Sciences, National Central University, Taoyuan, Taiwan*
[c] *Carbon Storage and Geothermal Research Center, National Central University, Taoyuan, Taiwan*
[d] *Department of Geosciences, National Taiwan University, Taipei, Taiwan*
[e] *Fabulous Power Co. Limited, Taipei, Taiwan*
[f] *Central Research Institute, Fukuoka University, Fukuoka, Japan*

ARTICLE INFO

Keywords:
Na/K geothermometer
Metapelite formations
Water-rock interaction
$T_{Na/K(albite\text{-}illite)}$

ABSTRACT

Taiwan is situated at one of the world's most active orogenic belts with arc-continent collision. This event resulted in the burial and uplift of mudstones along the continental margin, transforming them into metapelitic mountains. These mountains intercept rainfall and serve as the driving force for deep water circulation, enabling meteoric fluids to carry residual heat to the surface, thus giving rise to hot springs. The Taiwan orogenic belt is home to over 100 hot springs, and some of the hot spring reservoir temperatures such as Chingshui, Tuchang-Jentse, Lushan, Chihpon, and Chinlun exceeds 160 °C. Geothermal development in Taiwan has been carried out in such hot spring areas without any volcanic activities.

In order to assess reservoir temperatures and confirm the applicability of the Na/K geothermometer to such high temperature hot spring system, the concentrations of Na^+, K^+, and SiO_2 were analyzed from geothermal wells. Considering the mineral composition of metapelitic host rock, a new Na/K geothermometer is proposed based on equilibrium between albite and illite:

$$T > 180^{\circ}C,\ T(^{\circ}C) = \frac{2474}{\log\left(\frac{Na}{K}\right) + 3.73} - 273.15$$

This formula is only applicable in a reducing fluid and does not involve the formation of clay minerals except illite. It also requires several years to reach equilibrium. When using this formula to estimate reservoir temperatures, careful consideration of various conditions is necessary. It is advisable to incorporate both quartz geothermometer and down-hole temperature measurements for a more accurate assessment. Combining the Na/K geothermometer with the quartz geothermometer, along with other geochemical data such as Cl^-concentrations and δD and $\delta^{18}O$ of fluid, helps to understand whether hydrothermal fluids have undergone evaporation, dilution, and/or mixing processes.

1. Introduction

Most geothermal power plants are constructed on conventional geothermal systems, which are defined by their high enthalpy and high permeability. These systems are commonly found in areas characterized by active volcanism (Deon et al., 2012), recent plutonism (< 3Ma), and increased heat flow caused by extensional tectonics (Faulds et al., 2009; Moeck, 2014; Nukman and Moeck, 2013). However, there has been increasing interest in non-volcanic geothermal fields, particularly those in high-heat flow areas within orogenic belts, since the introduction of Enhanced or Engineered Geothermal Systems (EGS) (Moeck, 2014). In Taiwan, the geothermal fields associated with volcanic activity are mostly situated within national parks, such as the Tatun Volcano Groups. Consequently, the development of these fields involves navigating complex legal procedures. As a result, the extensive hot spring areas located in Taiwan's orogenic belts have emerged as an alternative

* Corresponding author.
E-mail address: yichialu@cc.ncu.edu.tw (Y.-C. Lu).

https://doi.org/10.1016/j.geothermics.2024.103133
Received 7 September 2023; Received in revised form 4 August 2024; Accepted 5 August 2024
Available online 17 August 2024

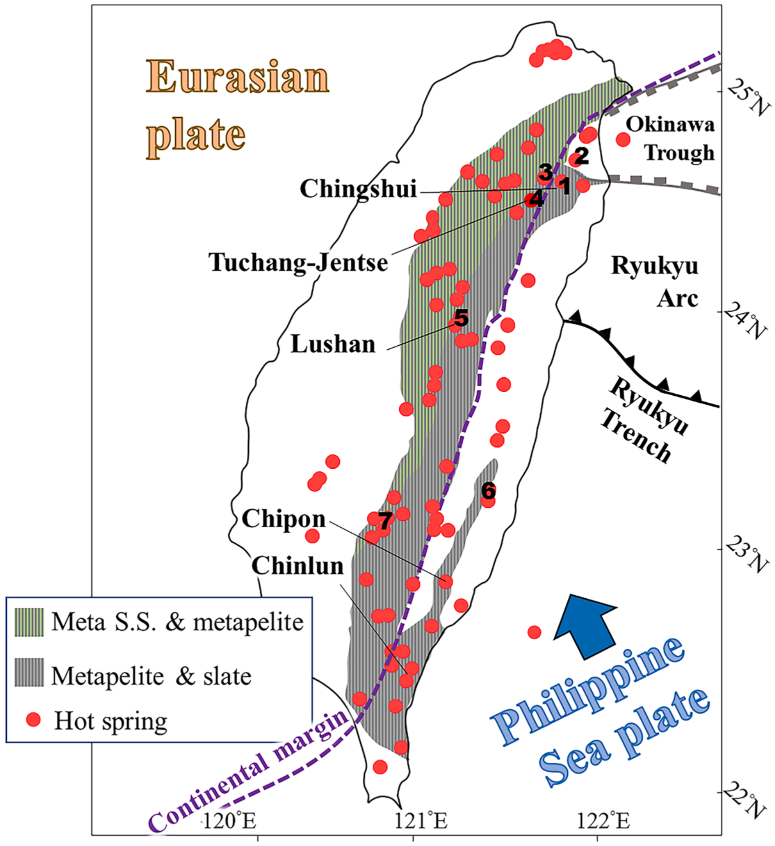

Fig. 1. The tectonic setting and the distribution of hot springs in Taiwan. The distribution of hot springs in Taiwan overlaps with the distribution of metapelite. These high-heat flow areas, formed by the rapid uplift of deeply buried continental margin sediments due to plate collision, constitute the primary regions for Taiwan's future geothermal development. The numbers on the figure correspond to the mineral content ratios of the metapelite in Table 3 for each geothermal field.

Table 1
The main geothermal areas in Taiwan within the metamorphic mudstone orogenic zone include Chingshui (Thermal manifestations, M.R.S.O., 1975; Well data, ITRI, 1994; Chemistry, Lu et al., 2017), Tuchang-Jentse (Thermal manifestations, Hsiao and Chiang, 1979; Well data, Jhan et al., 1986; Chemistry, ITRI, 1994), Lushan (Thermal manifestations and well data, Chang and Chiao, 1979; Hsiao et al., 1980), Chihpon (Thermal manifestations and well data, ITRI, 1994; Chemistry, data collected in this paper on 2020/12/17), and Chinlun (ITRI, 1994).

Thermal manifestations	Chingshui Boiling spring Travertine Boiling Spring Hot spring Fumaroles	Tuchang-Jentse Sinter Travertine Boiling spring Hot spring	Lushan Sinter Travertine Boiling spring Hot spring Fumaroles	Chihpon Hot spring Travertine	Chinlun Boiling spring Hot spring
Well name	IC-5	CPC-IT-2	NL-2	CPC—CP-1T	TCL-1
Well depth	2005 m	2277 m	501 m	1460 m	1000 m
Highest T	220 °C	219 °C	173 °C	182 °C (240 m)	159 °C
flow rate	61.3 ton/hr	118.8 ton/hr	33 ton/hr	40.3 ton/hr	20 ton/hr
Pressure	4.7 kg/cm^2	8.4 kg/cm^2	11 kg/cm^2	1.41 kg/cm^2	2.5 kg/cm^2
Steam ratio	10 %	22 %	3.4%		1.1 %
Geothermal area	1.3 km x 0.7 km	2 km x 2 km	2 km x 2 km (only Lushan) 6 km x 3 km (Include Lushan, Jingying, and Chunyang)	3 km x 0.6 km	4.5 km x 1.5 km
pH value	8.8	9.0	9.0	8.2	8.6
Fluid property	$NaHCO_3$	$NaHCO_3$	$NaHCO_3$	$NaHCO_3$	$NaHCO_3$
Na^+ (mg/L)	913	1031	763	719	554
K^+ (mg/L)	30	44.9	25.5	28.7	19
Ca^{+2} (mg/L)	0.8	1.7	2	0.72	1
Mg^{+2} (mg/L)	0.1	0.7	0.2	<0.1	1
HCO_3^-(mg/L)	2219	2196	2004	1739	1084
SO_4^{2-}(mg/L)	34	27.7	52.2	37.3	41
Cl^-(mg/L)	23	19	18	217	138
SiO_2 (mg/L)	418	389	216	172	174

and promising option for geothermal development to meet the growing demand for renewable energy.

From a tectonic perspective, Taiwan has been formed by the Penglai orogeny, an arc-continent collision that occurred around 5 million years ago (Byrne et al., 2011; Seno and Maruyama, 1984; Tsai et al., 1981; Yu and Chen, 1994). The Philippine Sea Plate continues to exert west-northwestward pressure on the Eurasian Plate, with a displacement rate of 4.9 to 8.5 cm/yr in the past few million years (Chen, 1982; Hsu et al., 2016; Lee, 1977; Liu, 1982, 2001; Shen et al., 2020; Yu et al., 2013). As a result, sedimentary deposits originally located on the continental shelf at the margin of the Eurasian continent since 15 Ma have been deeply buried to depths of up to 10 kms before uplifting (Chen and Wang, 1996). Eventually, these uplifted metapelite belts emerged at the surface during the late Pliocene (Chen and Wang, 1988b; Chen et al., 2019). Throughout this process, the geological layer has experienced a shortening of approximately 150–200 kms (Suppe, 1981). The mudstone and occasional sandstone layers have undergone transformation into metapelite, and even phyllite under metamorphic temperatures around 300 °C (Chen and Wang, 1996). The island has gradually taken shape, extending from north to south and from east to west (Ho, 1986; Lin, 1957; Teng, 1990, 1987). To date, the uplift rate of Taiwan is estimated to be approximately 5–7 mm/year (Ching et al., 2011), while the erosion rate is estimated to be around 3–6 mm/year, making it one of the highest in the world (Dadson et al., 2003; Nisbet and Fowler, 1982).

These uplifted metapelite, resulting from mountain building, cover approximately 3/5 of Taiwan's. They extend for a distance of 330 km from north to south and 40–70 km wide, with the highest elevation of almost 4000 m above sea level (Chen, 2016). The topographic head differential in these mountainous regions provides the hydraulic force necessary to drive meteoric water deep into the fault zone, where it is heated. This heated water then ascends through fracture zones as hot springs (Chen, 1975, 1985). It is estimated that there are over 100 hot springs located here, including the places with great geothermal potential, the Chingshui geothermal field (Chang et al., 2014; Hsiao and Chiang, 1979; Ho et al.,2014; Hsieh et al.,2021; Lu et al., 2017; 2018; 2020; M.R.S.O.,1975; Tong et al., 2008), Tuchang-Jentse geothermal field (Chan et al.,1986; Chen et al.,2021; 2023; Hsiao and Chiang, 1979; Lin and Lin, 1995; Lu et al., 2023; M.R.S.O., 1975; Tseng, 1978), Lushan geothermal field (Chang and Chiao, 1979; Hsiao et al., 1980), Chihpon geothermal field (Anon., ITRI,1994), and Chinlun geothermal field, etc. (ITRI,1994; Fig. 1 and Table 1).

When assessing the geothermal potential of these locations, reliable geological thermometers play a crucial role in estimating reservoir temperatures. The SiO_2 geothermometer has been proven to be suitable for metapelite formations in Taiwan (Chen, 1985; Huang et al., 2018). Additionally, due to the C_{Na}/C_K ratio is independence from spring water evaporation or dilution (Ellis and Wilson, 1960; Ellis and Mahon, 1964), we aim to incorporate the Na/K geothermometer as an additional reference alongside the SiO_2 geothermometer for estimating reservoir temperatures.

However, the applicability of the Na/K geothermometers in the Taiwan orogenic belt has long been debated. The commonly used formula based on the albite and orthoclase equilibrium (Arnorsson et al., 1983; Can, 2002; Diaz-Gonzalez et al., 2008; Fournier, 1977, 1979; Fournier and Rowe, 1966; Fournier and Truesdell, 1974; Nieva and Nieva, 1987; Reyna-Avilez et al., 2023; Tonani, 1980; Verma and Santoyo, 1997; Valencia-Cabrera et al., 2022; White, 1970) is not suitable for metapelite formations where K-feldspar is absent. Chen (1985) proposed an albite-muscovite equilibrium formula for the Na/K geothermometer in metapelite formations. However, 60-day metapelite-fluid interactions have shown a reverse relationship between the Na/K geothermometer and experimental temperature (Huang et al., 2018).

This study commences by providing a comprehensive comparison of the reservoir characteristics of the metapelitic geothermal field in Taiwan orogenic belt with those of other orogenic belts around the world. The subsequent steps involve an attempt to develop a dedicated Na/K geothermometer for the metapelitic geothermal field. This is achieved by analyzing the concentrations of Na^+, K^+, and SiO_2 collected from geothermal wells and then comparing the results with previously established Na/K geothermometers. Additionally, the minerals involved in the equilibrium of water-rock reactions are thoroughly discussed. Ultimately, the study concludes by summarizing and evaluating the applicability of the Na/K geothermometer for the Taiwan metapelitic geothermal field.

2. Analytical methods

2.1. Water chemistry analysis

A total of 139 samples from 33 deep wells are collected for the feasibility test of Na/K geothermometer. Among them, 61 samples are from the Chingshui geothermal field, 66 are from the Tuchang-Jentse geothermal field, 6 are from the Lushan geothermal field, 5 samples are from the Chihpon geothermal field, and 1 is from the Chinlun geothermal field.

To compare the differences in fluid properties between metapelitic reservoirs and surface conditions, this study examines 9 surface hot spring samples with temperatures ranging from 33 to 99 °C. Of these, 6 are from Chingshui, and 3 are from the Lushan geothermal field.

Among these fluid chemical data, 88 records are from the large-scale geothermal exploration across Taiwan from 1974 to 1986 (Chen, 1985; Tseng, 1978; ITRI, 1994). 3 records are from the 2007 survey conducted by the Central Geological Survey (Chen, 2011), 2 records are from well renovation in 2008 and 2009 (ITRI, 2010, 2012), and the rest comes from the analysis of the Department of Geology of National Taiwan University in this study and Lu et al.(2020). The 1970s data represents the first collection of thermal fluids in the geothermal area of Taiwan, while the rest involves the re-collection of reservoir geothermal water after a resting period of over 24 years (following the closure of the Chingshui geothermal power plant and the Tuchang-Jentse geothermal power plant in 1993).

The geothermal well temperatures are indicated as follows: HT for the highest temperature, WB for the bottom temperature, and WH for the well head temperature. The pH values are denoted as R for measurements taken after indoor cooling, and F for measurements taken directly during sampling. The hot fluids were filtered through 0.22 μm cellulose filters in the field and stored in well-sealed 100 mL plastic bottles. Three types of samples were taken at each location: a filtered sample for carbonate titration, isotope and anion analysis; a 1/10 diluted solution for silica analysis, and a sample with HCl added for cation analysis.

Compositions of carbonates and bicarbonates were analyzed by the 877 Titrino Plus made by Metrohm, Switzerland. The concentrations of anions and some of the cations, potassium, sodium, calcium, and magnesium were analyzed by 883 Intelligent Ion Chromatography made by Metrohm. The concentration of SiO_2 was analyzed using the Ultima 2 model of Inductively Coupled Plasma-Atomic Emission Spectroscopy (ICP-AES) produced by HORIBA at Department of Geosciences, National Taiwan University.

For deriving an empirical Na/K geothermometer in metapelite formation, we use the silica temperatures in quartz instead of maximum downhole temperature for the following three reasons: (1) the measurement of well temperatures involves considerations such as the time elapsed after drilling and whether temperature equilibrium has been achieved. However, earlier reports often failed to provide clear explanations in this regard. Furthermore, some data represent the highest temperature, while others represent the bottom temperature or even the well head temperature. Therefore, it is challenging to use them as reference temperatures for Na/K geothermometers; (2) different water temperatures may come from different fractured systems in the same well, resulting the average temperature lower than maximum downhole

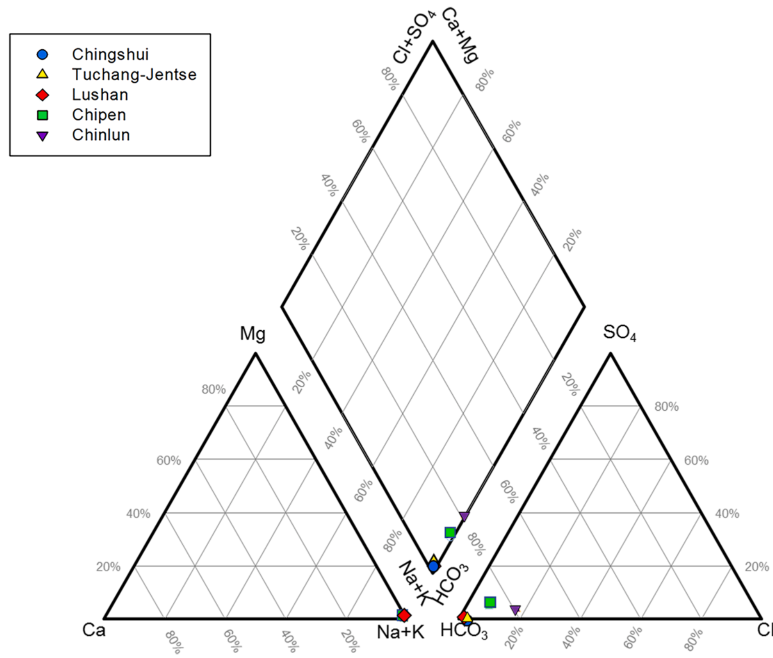

Fig. 2. The Piper diagram reveals that the hot springs in the Taiwan orogenic belt belong to the bicarbonate-sodium type. Chipen and Chinlun exhibit slightly higher chloride ion concentrations compared to Chingshui, Tuchang-Jentse, and Lushan.

temperature; and (3) the silica is dissolved in water, which records water temperature precisely.

The quartz geothermometer for boiling spring under condition of maximum steam loss (Fournier, 1977):

$$T(^{\circ}\mathrm{C}) = 1522/(5.75 - \log(\mathrm{SiO_2})) - 273.15$$

2.2. Mineral analysis

In order to understand the minerals and their proportions within the metapelitic formations in the Taiwan orogenic belt, we collected host rocks from 7 geothermal fields in the following order as labeled in Fig. 1: 1.Chingshui, 2.Hongchailin, 3.Pengpeng, 4.Tuchang-Jentse, 5.Lushan, 6.Hongyegu, and 7.Baolai for X-ray diffraction (XRD) analyses. The measurements were conducted using the D2-PHASER produced by Bruker at the prestigious Carbon Storage and Geothermal Research Center of National Central University, Taiwan. The mineral semi-quantitative calculation was determined by integration of the peaks for each mineral using Match! Powder Diffraction Analysis Software and the integration areas were summed to reach a total of 100 % as the calculation basis.

To gain a comprehensive understanding of the morphology of minor minerals and verify the elemental composition within metapelite, we utilized the FEI QUANTA200 scanning electron microscope (SEM) equipped with a Back-scattered Electron Detector (BSE) and conducted Energy Dispersive Spectrum (EDS) analyses. This research was carried out at the Department of Geosciences, National Taiwan University.

3. Results and discussion

3.1. The thermal fluid characteristics of Taiwan matapelitic geothermal field

Geochemically, the hot fluids in the metapelitic geothermal field of Taiwan orogenic belt belong to the sodium bicarbonate type (Fig. 2). Chen (1982) proposed that the heat source of hot fluid originated from the residual heat of rock formations. The meteoric water infiltrated downward, was heated by the surrounded rocks with a high geothermal gradient, then rose to the shallower reservoirs or to the surface as hot springs through regional faults or fractured systems. The hydrogen and oxygen isotopic compositions suggested that the thermal fluids came from the deep circulation of meteoric water, and indicated the hot fluids come from a meteoric origin with a recharge area located at an altitude above 1000 m (Liu et al., 1990, 1982; Lu et al., 2020, 1982; Yui et al., 1993).

The concentration of HCO_3^- in Chingshui, Tuchang-Jentse, and Lushan is close to 2200 mg/L (Table 1), while Chihpon, and Chinlun have bicarbonate ion concentrations of over 1000 mg/L. The concentration of Na^+ in Chingshui and Tuchang-Jentse is around 1000 mg/L, while in other areas, it is above 500 mg/L. In contrast, the concentration of sulfate and chloride ions in the metapelitic geothermal field is quite low. The SO_4^{2-} concentration ranges from 20 mg/L to 60 mg/L, while the Cl^- concentration in the Chingshui, Tuchang-Jentse, and Lushan is below 25 mg/L. In the Chihpon and Chinlun, the Cl^- concentration ranges from 130 mg/L to 220 mg/L (Table 1).

As there is no association with hydrothermal and magmatic activity, the absence of sulfate and chloride from magmatic sources is expected. In the metapelitic geothermal field of the Taiwan orogenic belt, the high concentration of bicarbonate may partly originate from water-rock reactions involving hydrothermal activity (Huang et al., 2018). In the northern regions of Taiwan, Chingshui and Tuchang-Jentse, there may also be additional contribution from the decarbonation of marble beneath the metamorphic mudstone, as supported by carbon isotope evidence (Lu et al., 2017). The elevated concentration of Na^+, on the other hand, is derived from the dissolution of albite or plagioclase under the influence of bicarbonate ions (Chen, 1985). The slightly higher Cl^- concentration in the southern region may be related to the presence of brine in the geological formations and/or from the water-rock interaction of intrusion diabase, which was reported appeared at the Chihpon geothermal field (ITRI, 1994).

From Table 1 and Appendix-1, it can be observed that the Chingshui, Tuchang-Jentse, Lushan, Chihpon, and Chinlun exhibit extremely high geothermal gradients inside 2300 m depth. Downhole data indicates temperatures up to 220 °C, 219 °C, 173 °C, 182 °C, and 159 °C with productions of 61 tons/hr, 119 tons/hr, 33 tons/hr, 40 tons/hr, and 20 tons/hr, respectively. These high enthalpy and $NaHCO_3$-type fluid characteristics are more similar to Eastern Tibetan Plateau geothermal

Table 2
Table 2 is a simplified version of Appendix 1, comparing the measured well temperatures (highest temperature - HT, bottom temperature - WB, and head temperature - WH), T_{quartz}, previously published $T_{Na\text{-}K}$ based on equilibrium with Na-feldspar and K-feldspar, and the $T_{Na\text{-}K}$ based on equilibrium with albite-illite/muscovite in this study. An asterisk (*) denotes wells where the temperature is below 180 °C and the formula is not applicable.

Location	Well No.	Year	Well depth (m)	Well T (°C)	HCO_3^- (mg/L)	Cl^- (mg/L)	SO_4^{2-} (mg/L)	Na^+ (mg/L)	K^+ (mg/L)	SiO_2 (mg/L)	Quartz adiabatic	Na/K Fournier 1979	Na/K Truesdel 1976	Na/K Giggenbach 1988	Na/K Tonani 1980	Na/K Nieva & Nieva 1987	Na/K Arnorsson 1983	Na/K This study
Chingshui	IC-01	1976	450	146 (HT)	1943	14.1	52.0	826	22.0	179	162*	125	79	145	102	114	90	193*
Chingshui	IC-02	1976	450	175 (HT)	2121	18.7	23.9	866	33.0	223	174*	146	103	165	128	135	114	207*
Chingshui	IC-04	1976	1505	201 (WB)	2619	18.3	32.0	1095	36.0	342	200	137	92	157	117	126	104	201
Chingshui	IC-05	2017	2005	220 (WB)	2452	13.8	16.5	910	38.4	408	212	153	110	172	137	141	121	212
Chingshui	IC-09	2017	2079	205 (WB)	3001	9.17	18.8	1102	38.3	329	198	141	96	160	121	129	107	204
Chingshui	IC-12	1978	2003	223 (WB)	2453	20.0	38.0	1128	50.0	428	215	156	114	175	141	144	124	214
Chingshui	IC-13	2009	2020	219 (WB)	1367	16.1	13.0	1040	49.8	379	207	161	120	180	147	149	130	217
Chingshui	IC-14	2017	2003	215 (WB)	2367	14.9	33.7	811	43.6	388	208	169	129	187	158	157	139	222
Chingshui	IC-16	2017	3000	225 (WB)	2483	15.3	14.2	1025	46.4	418	213	157	116	176	143	145	126	214
Chingshui	IC-19	2007	1227	206 (HT)	1890	15.0	22.0	1160	32.5	324	197	128	82	148	105	117	93	195
Chingshui	R1	2020	363	154 (WH)	2391	26.1	16.3	1054	58.2	347	201	171	131	189	160	159	141	223
Chingshui	R3	2021	337	154 (WH)	2495	12.3	12.2	878	32.0	237	178*	143	100	163	125	132	111	206*
Chingshui	R5	2021	500	156 (WH)	2446	28.5	12.4	1087	47.5	264	184	155	113	174	139	143	123	213
Tuchang-Jentse	IT-1	1974	161	163 (WB)	2822	32.6	29.7	1093	22.8	254	182	112	64	132	86	101	76	184
Tuchang-Jentse	IT-2	1974	240	171 (WB)	2323	42.5	33.7	1153	23.0	258	183	109	61	130	83	98	73	182
Tuchang-Jentse	IT-3	1975	445	173 (WB)	2665	27.7	35.7	1115	22.5	260	183	110	62	130	84	99	74	183
Tuchang-Jentse	IT-4	1975	280	144 (WB)	2110	14.6	18.5	841	14.0	163	157*	100	51	121	72	89	63	176*
Tuchang-Jentse	IT-5	1976	311	143 (WB)	2029	15.6	37.0	874	15.0	188	165*	101	53	122	74	91	65	177*
Tuchang-Jentse	IT-8	1976	1503	169 (HT)	2369	19.2	45.6	1105	23.0	238	178*	111	64	132	86	101	76	184*
Tuchang-Jentse	IT-11	1984	525	175 (HT)	2639	22.0	18.0	1113	19.7	255	182	103	55	124	76	92	67	178
Tuchang-Jentse	IT-12	1985	505	160 (HT)	2672	21.0	13.0	1138	26.4	335	199	117	70	138	93	106	82	188
Tuchang-Jentse	IT-13	1986	556	171 (HT)	2747	25.0	23.0	1058	18.4	217	173*	102	54	123	75	92	66	178*
Tuchang-Jentse	CPC-IT-1	2018	2200	136 (WH)	2769	20.5	8.27	974	33.8	391	209	140	96	160	121	129	107	204
Tuchang-Jentse	CPC-IT-2	2016	2277	194 (WB)	2898	19.0	39.5	1060	79.8	508	227	194	159	211	191	181	168	237
Tuchang-Jentse	CPC-ZJ-14	2021	2000	172 (HT)	2019	6.45	54.3	854	19.0	144	151*	115	68	135	90	104	79	186*

(continued on next page)

Table 2 (*continued*)

Location	Well No.	Year	Well depth (m)	Well T (°C)	HCO_3^- (mg/L)	Cl^- (mg/L)	SO_4^{2-} (mg/L)	Na^+ (mg/L)	K^+ (mg/L)	SiO_2 (mg/L)	Quartz adiabatic	Na/K Fournier 1979	Na/K Truesdel 1976	Na/K Giggenbach 1988	Na/K Tonani 1980	Na/K Nieva & Nieva 1987	Na/K Arnorsson 1983	Na/K This study
Tuchang-Jentse	CPC-ZJ-15	2021	1500	166 (HT)	2471	12.4	29.7	804	23.1	218	173*	129	84	149	107	118	95	196*
Lushan	NL-1A	1978	227	168 (HT)	2096	15.0	55.0	796	25.0	281	188	134	89	154	114	123	101	200
Lushan	NL-2	1978	501	173 (HT)	1874	15.0	38.0	763	25.5	216	172*	138	94	158	118	127	105	202*
Lushan	NL-3	1978	516	98 (HT)	4431	21.0	43.0	1664	15.0	75	120*	72	22	93	39	62	34	155*
Lushan	NL-4	1979	300	115 (HT)	2129	0.00	67.0	740	5.00	131	146*	60	9	81	26	50	22	146*
Lushan	NL-5	1979	300	149 (HT)	1939	7.00	21.0	710	6.00	118	141*	69	19	90	36	59	31	153*
Chihpon	TC-1	1979	500	122 (HT)	1407	76.0	72.0	603	6.00	118	141*	76	26	97	44	66	38	158*
Chihpon	TC-2	1980	493	125 (HT)	1672	81.0	78.0	749	6.00	135	147*	67	17	88	34	57	29	151*
Chihpon	TC-3	1980	500	125 (HT)	1994	179	56.0	976	10.0	180	162*	77	27	99	46	67	40	159*
Chihpon	TC-4	1980	500	155 (HT)	1648	195	52.0	863	16.0	216	172*	105	57	126	78	95	69	180*
Chihpon	TC-5	1980	500	159 (HT)	1585	232	43.0	847	18.0	223	174*	113	65	133	87	102	77	185*
Chinlun	TCL-1	1980	1000	159 (HT)	1084	138	41.0	554	19.0	174	161*	140	95	159	120	128	106	203*

belt (Shi et al., 2017) and Alpine Fault of Southern Alps, New Zealand (Reyes et al., 2010), but differ from those orogenic geothermal fields of deep reservoir, high Cl^- and average geothermal gradients, i.e. Alps orogenic belts, such as the Grimsel Pass geothermal system (Diamond et al., 2018) and Lavey-les-Bains (Sonney and Vuataz, 2009) in Switzerland, the Molasse basin in Germany (Cacace et al., 2013), the Rocky Mountains in Canada (Grasby and Hutcheon, 2001), the Pyrenees in Spain within the Hercynian orogeny of the Alpine belt (Asta et al., 2010), and the Qilian Mountains in China (Stober et al., 2016). However, both the Tibetan Plateau and the Alpine Fault in New Zealand have granite intrusions and an abundance of K-feldspar, which acts as a material in equilibrium with plagioclase at different temperatures. Therefore, the $T_{Na/K}$ presented by Giggenbach (1988) are similar to the T_{quartz} (e.g., the T_{quartz} is 230 °C, and the $T_{Na/K}$ is 215 °C at Yidun-Litang, data from Shi et al., 2017). In comparison, there is a significant $T_{Na/K}$ and T_{quartz} difference, up to +57 °C, in the Taiwan orogenic belt (Table 2 and Appendix-1). in other words, whether in terms of applicable conditions or actual measurements, the $T_{Na/K}$ (albite- K-feldspar) is not suitable for the metapelite geothermal fields in Taiwan.

3.2. Na/K geothermometer in the metapelitic geothermal field of Taiwan orogenic belt

The concentrations of Na^+, K^+, SiO_2, calculated SiO_2 temperature, and actual measured temperature of geothermal wells are presented in Appendix 1. Fluids from the Chingshui and Tuchang-Jentse geothermal fields exhibit the highest T_{quartz}, followed by Lushan one, and finally Chihpon and Chinlun. The data plotted on Na-K-Mg ternary diagram (Giggenbach, 1988) exhibit either equilibration or partial equilibration in Fig. 3.

Plots of log(Na/K) and $10^3/T_{SiO2}(K)$ of deep well fluids are shown in Fig. 4. It shows better correlations of log(Na/K) based on the quartz geothermometer above 180 °C than those below 180 °C. It is not surprised, according to the water-slate interaction experiment by Huang et al. (2018), the deviation >180 °C is only 1–6 °C in the quartz geothermometer, but 20–30 °C when <180 °C due to its polymorph phase transition. The equilibrium temperature derived from log (Na/K) and $10^3/T_{quartz}(K)$ can be described by the equation:

$$T > 180^{\circ}C \quad T(^{\circ}C) = [2474 / \log(Na + K) + 3.73] - 273.15 \quad R^2 = 0.71$$

$$T < 180^{\circ}C \quad T(^{\circ}C) = [1430 / \log(Na / k) + 1.53] - 273.15 \qquad R^2 = 0.32$$

Plotting the Na/K geothermometer temperatures estimated using the formula for ones above 180 °C on the horizontal axis and the quartz geothermometer ones on the vertical axis (Fig. 5) reveals a good correlation between those two. Most of the calculated errors between $T_{Na\text{-}K}$ and T_{quartz} are <8 °C. When comparing our formula with previously published Na/K geothermometer (Fig. 6), it is evident that, at the same C_{Na}/C_K ratio, our formula produces lower temperatures than Chen (1985), but higher temperatures than other geothermometers based on Na-feldspar and K-feldspar equilibrium (Arnorsson et al., 1983; Can, 2002; Diaz-Gonzalez et al., 2008; Fournier, 1979; Nieva and Nieva, 1987; Tonani, 1980; Verma and Santoyo, 1997). We infer that the limited drilling data available for Chen (1985), with only two data points from geothermal wells and the remainder from spring water adjusted for dilution calibration, resulted in significantly deviated temperatures. Obviously, geothermometers based on Na-feldspar and K-feldspar equilibrium provide lower temperature estimates and are not suitable for the metapelitic geothermal field of the Taiwan orogenic belt.

3.3. Na/K geothermometer based on equilibrium between albite and illite

The Taiwan metapelitic formation comprises several key minerals listed in order of abundance: quartz (37–76 %), illite/muscovite (8–56

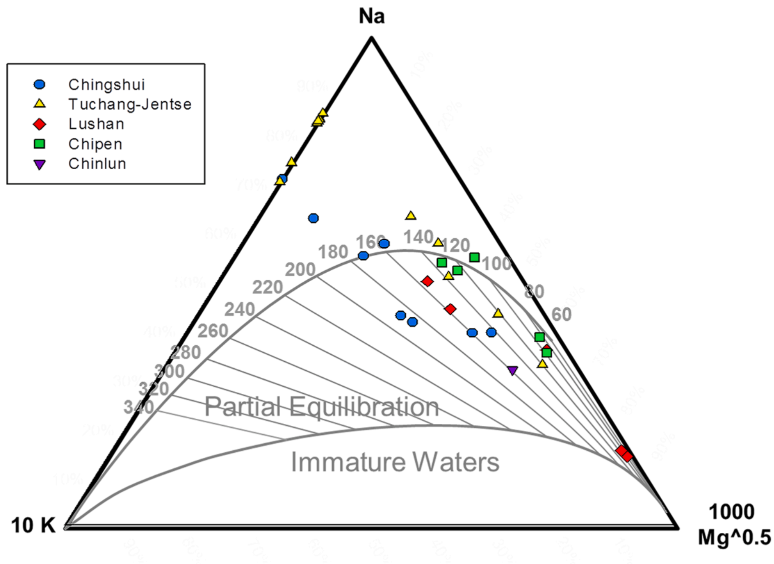

Fig. 3. The Na-K-Mg diagram (Giggenbach, 1988) indicates that the hot fluids in the Taiwan orogenic belt are in equilibrium or partial equilibrium with Na-feldspar and K-feldspar.

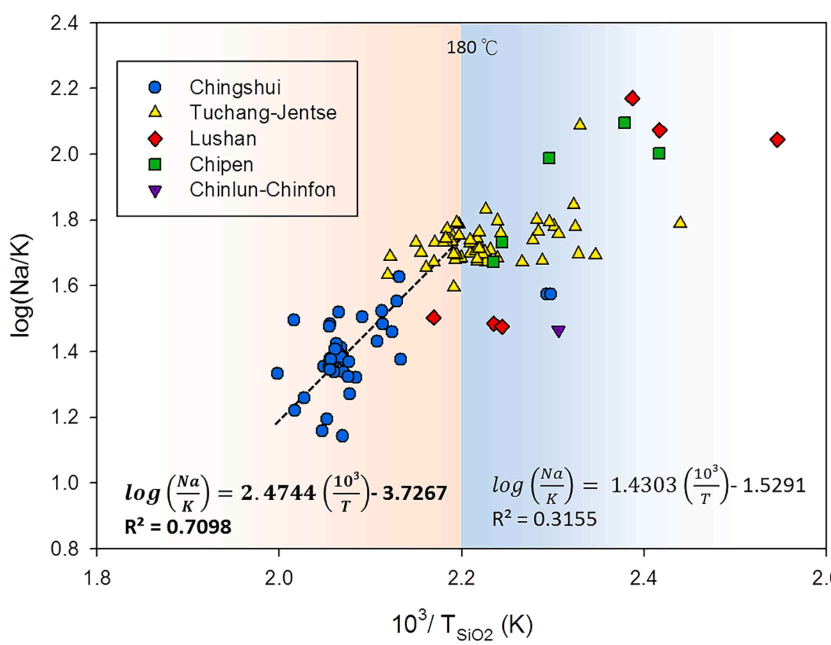

Fig. 4. The log(C_{Na}/C_k) and $10^3/T_{qtz}$ >2.2 exhibit a stronger correlation, with an R^2 value of up to 0.71, while the correlation with $10^3/T_{qtz} < 2.2$ is lower, with an R^2 value of only 0.32. This indicates that the Na/K geothermometer in the mata-mudstone of Taiwan is only applicable for temperatures higher than 180 °C.

%), chlorite (1–26 %), and feldspar (1–12 %). These proportions display significant variations depending on the sampling locations (Table 3 and Appendix 2). In other words, the host rocks in the Taiwan orogenic belt most likely involved in Na/K fluid-rock equilibrium is feldspar and illite. Furthermore, assuming that the hydrothermal fluid in this context closely resembles an ideal solution, we use a pH value of 6.39 to calculate the activity of H^+(The pH values measured on the surface mostly range between 8.0 and 9.6; however, these readings are the result after the removal of dissolved carbon dioxide from water. Hsieh et al., 2021 tested Chingshui well IC-19, with the pH value at the wellhead recorded as 8.97 and the pH value underground as 6.39 by the downhole sampling equipment). Plotting the ratios [aNa^+/aH^+] and [aK^+/aH^+] of the well's hot fluid onto the calculated equilibrium phase diagram of the Na_2O–Al_2O_3–SiO_2–K_2O–H_2O system reveals that the majority of samples align with the equilibrium lines of albite and illite (Fig. 7).

The primary participants in the sodium-potassium equilibrium are likely to be feldspar and illite, aligning with Chen's argument proposed in 1985:

$$3\ \text{albite} + 2H^+ + K^+ \leftrightharpoons 3\ Na^+ + \text{illite} + 6\ \text{Quartz}$$

The activity diagram(Fig. 7) for Na^+–K^+ (Na_2O-–Al_2O_3–SiO_2–K_2O–H_2O) shows that a small portion of the data does not lie on the equilibrium of albite and illite, but instead falls on the equilibrium of albite and Na-montmorillonite. This suggests that the Na/K geothermometer in the metapelite may also involve water-rock interaction with albite, K-mica, Na-montmorillonite, and even kaolinite. In the following, we will combine the hydrochemistry of hot springs and downhole core analysis of Taiwan metapelite to investigate the

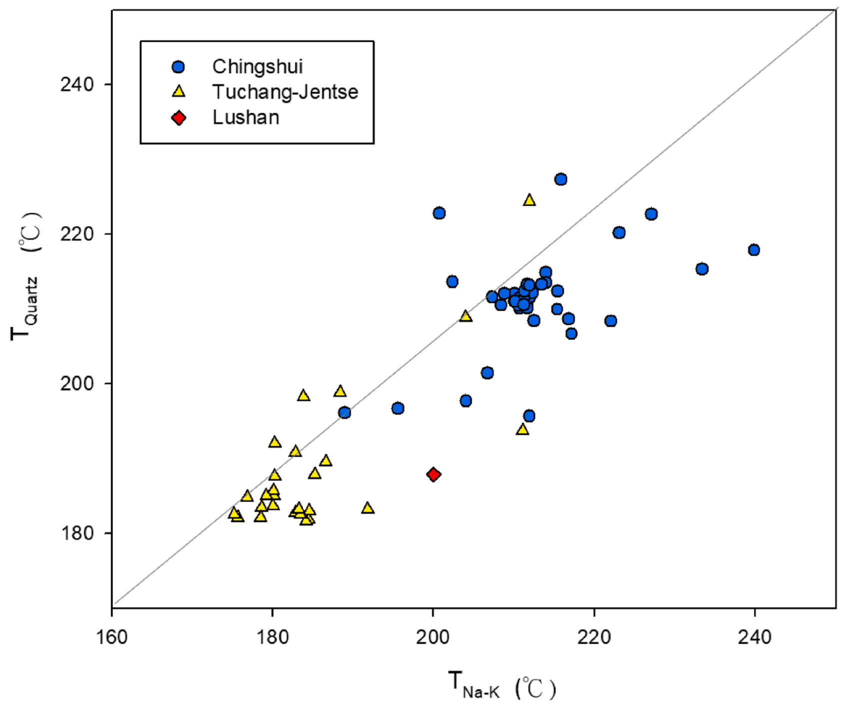

Fig. 5. The feldspar-illite in equilibrium of T_{Na-K} with T_{qtz} exhibit a correlation coefficient (R^2) of approximately 0.71.

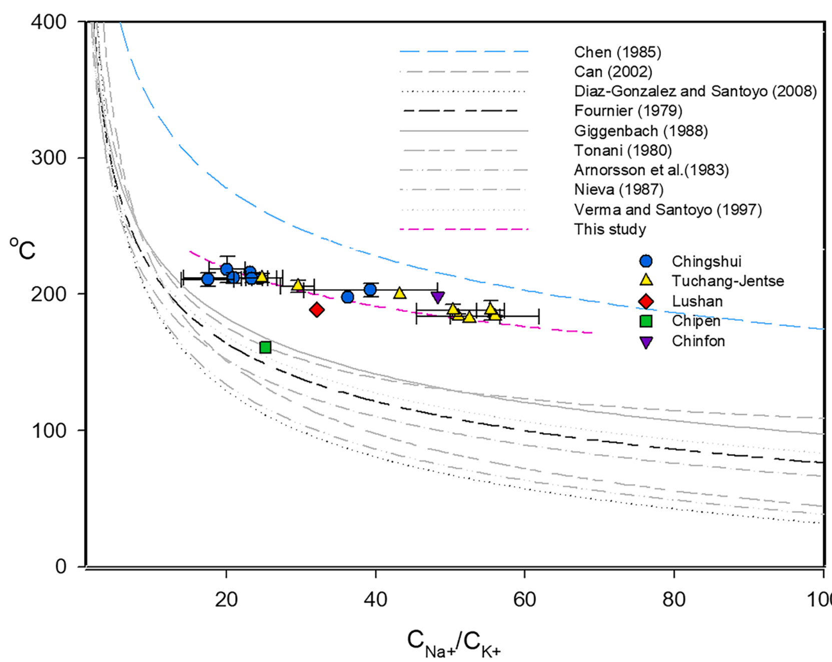

Fig. 6. The Na/K geothermometer based on albite -illite in this study (pink) is compared to Chen (1985, blue) and other Na-Feldspar and K-feldspar geothermometers (gray).

influence of redox on the Na/K geothermometer.

3.4. Redox affects the Na/K geothermometer

It is evident that the mineral compositions of surface and subsurface exhibit different characteristics. Here, a conceptual model is used to illustrate this (Fig. 8). In deep cores extracted from production wells, minimal alteration was observed, despite the surrounding veins in the host rock (Lu et al., 2017). Euhedral or framboidal pyrite crystals are widely distributed within the metapelite (Fig. 9A and B), including inside calcite/quartz veins, indicating a reducing environment in the reservoir. This suggests only a simple albite -illite reaction occurs, allowing for a stronger correlation with temperature. Another piece of evidence for reducing reservoirs comes from the Chingshui boiling springs. These springs, being powerful upwellings, closely resemble the conditions of the reservoir fluids, displaying an Eh of −492.5 mV (Table 4), directly indicative of a reducing environment.

On the contrary, the surface hot springs exhibit Eh values reaching up to +105 mV, reflecting an oxidizing environment. These steaming grounds and hot springs are indicative of an oxidizing environment,

Table 3
Semi-quantitative mineral content of the host rocks in different metapelitic geothermal fields. Samples marked with an asterisk (*) are from Huang et al., 2018.

	Illite	Chlorite	Quartz	Feldspar	Pyrite
ICDD card	02–0050	02–0028	75–0443	89–0710	01–089
2-theta	8.9 °	12.6 °	26.6 °	27.6 °	33.1 °
1. Chingshui-1	56 %	1 %	37 %	5 %	<0.1 %
1. Chingshui-2	9 %	19 %	59 %	12 %	<1 %
1. Chingshui-3 *	19 %	23 %	50 %	7 %	<0.1 %
1. Chingshui-4 *	11 %	25 %	53 %	10 %	<0.1 %
1. Chingshui-5 *	12 %	19 %	59 %	11 %	<0.1 %
2. Hongchailin	42 %	26 %	25 %	8 %	<0.1 %
3. Pengpeng	8 %	7 %	76 %	9 %	<0.1 %
4. Tuchang-Jentse	18 %	8 %	73 %	1 %	<0.1 %
5. Lushan	41 %	14 %	42 %	3 %	<0.1 %
6. Hongyegu	18 %	13 %	64 %	5 %	<0.1 %
7. Baolai	22 %	2 %	63 %	8 %	<0.1 %

suggesting they could be either steaming heated meteoric fluids or a mixture of oxidized meteoric water and reduced hydrothermal fluid (Fig. 8). Under oxidizing conditions, the pyrite in the host rock decomposes, leading to a significant increase in iron and sulfate ions in the fluid (Table 4). The oxidation process once again causes the iron ions in the water to precipitate as Fe_2O_3, explaining why some surface springs display a distinct iron rust coloration.

The sulfate ions resulting from the decomposition of pyrite enhance surface hydrothermal alteration and lead to the formation of various sulfide minerals, such as gypsum, pure sulfur, and even indicative minerals like jarosite $KFe_3(OH)_6(SO_4)_2$(Appendix-2), which can be found in the Chingshui steaming ground. According to the dissolution experiment of alumina-silicate parent rocks, clay dissolved faster than feldspar (Lo et al., 2017), implying that clay minerals are more easily equilibrated with aqueous solution than feldspar in a hydrothermal system. The equilibrium of the Na/K reactions involved may include:

Illite and alunite:

$$KAl_3Si_3O_{10}(OH)_2 + 4H^+ + 2\,SO_4^{2-} \leftrightharpoons KAl_3(SO_4)_2(OH)_6 + 3\,SiO_2$$

Illite and kaolinite:

$$KAl_3Si_3O_{10}(OH)_2 + 2H^+ + 3\,H_2O \leftrightharpoons 3\,Al_2Si_2O_5(OH)_4 + 2\,K^+$$

Kaolinite and alunite:

$$3\,Al_2Si_2O_5(OH)_4 + 2\,K^+ + 6\,H^+ + 4\,SO_4^{2-} \leftrightharpoons 2KAl_3(SO_4)_2(OH)_6 + 6\,SiO_2 + 3\,H_2O$$

Albite and Na-montmorillonite:

$$1.17\,NaAlSi_3O_8 + H^+ \leftrightharpoons 0.5Na_{.33}Al_{2.33}Si_{3.67}O_{10}(OH)_2 + 1.67SiO_2 + Na^+$$

kaolinite and Na-montmorillonite

$$3\,Na_{.33}Al_{.33}Si_{3.67}O_{10}(OH)_2 + H^+ + 3.5\,H_2O \leftrightharpoons 3.5\,Al_2Si_2O_5(OH)_4 + 4SiO_2 + Na^+$$

Due to the involvement of various clay minerals and the mutual interaction and thermodynamic equilibrium between albite and these clay minerals, the C_{Na}/C_K ratio is unable to exhibit a well-correlated trend with temperature.

Huang et al. (2018) conducted 5–60 day water-rock reaction experiments to simulate the interaction between metapelite and hot fluids. They measured the changes in sodium and potassium in the fluids and the secondary minerals formed after the reactions. However, this

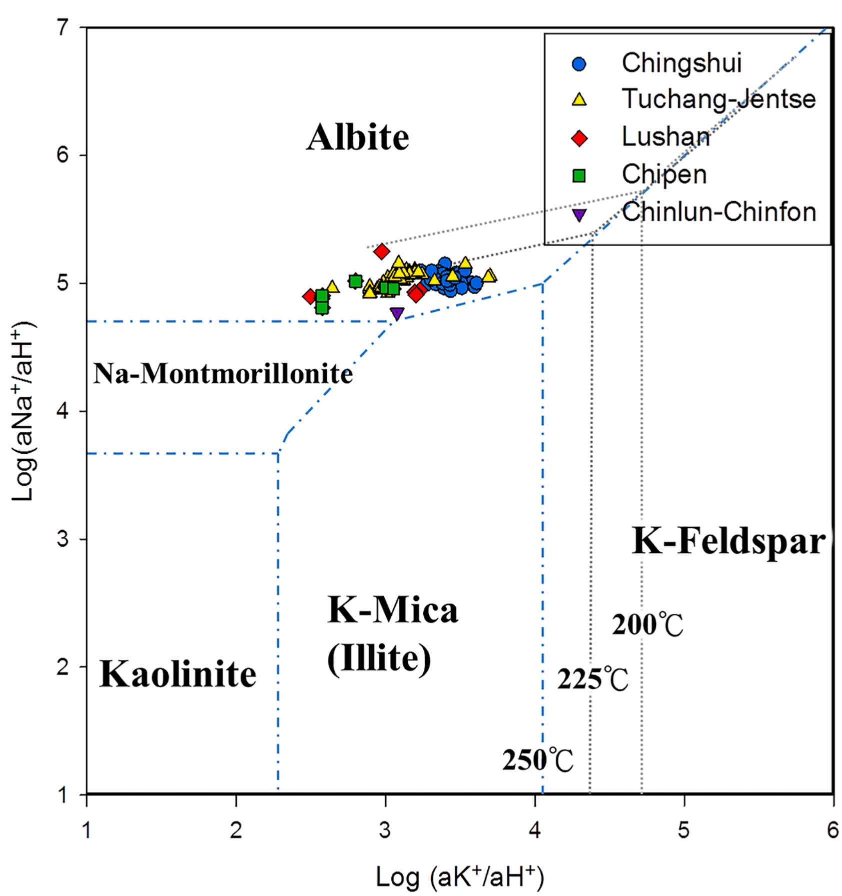

Fig. 7. Activity diagram for Na^+–K^+ (Na_2O–Al_2O_3–SiO_2–K_2O–H_2O) from geothermal well fluids in Chingshui, Tuchang-Jentse, Lushan, Chipen, and Chinlun-Chinfon, respectively. Most of the data lie on the equilibrium line between albite and illite.

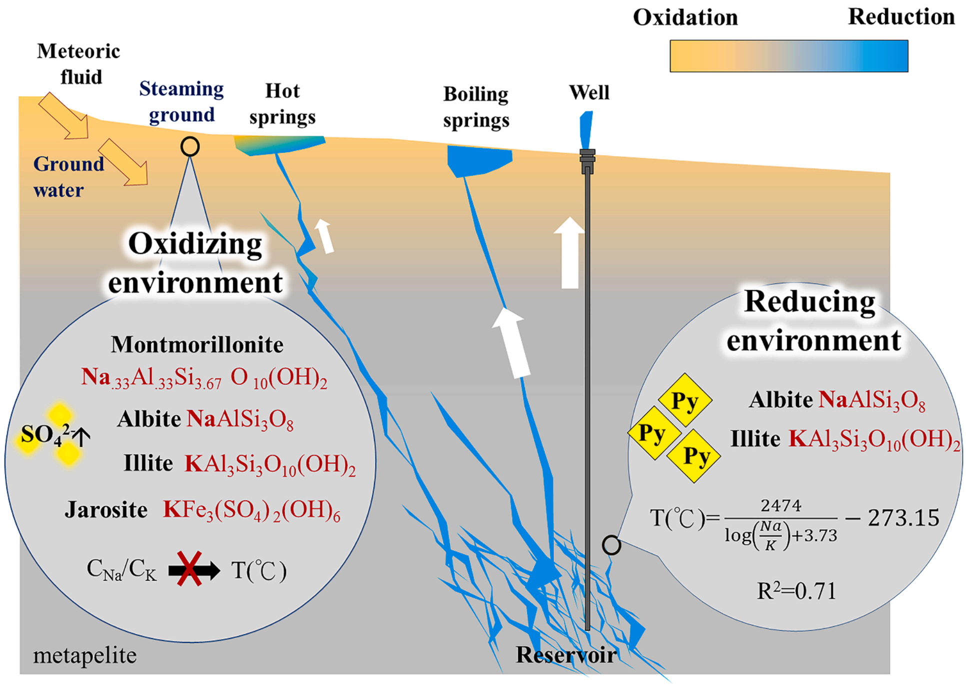

Fig. 8. The conceptual model illustrates how varying oxidation and reduction states result in different expressions of mineral assemblages and the equilibrium of C_{Na}/C_K with temperature in metapelitic non-volcanic geothermal fields.

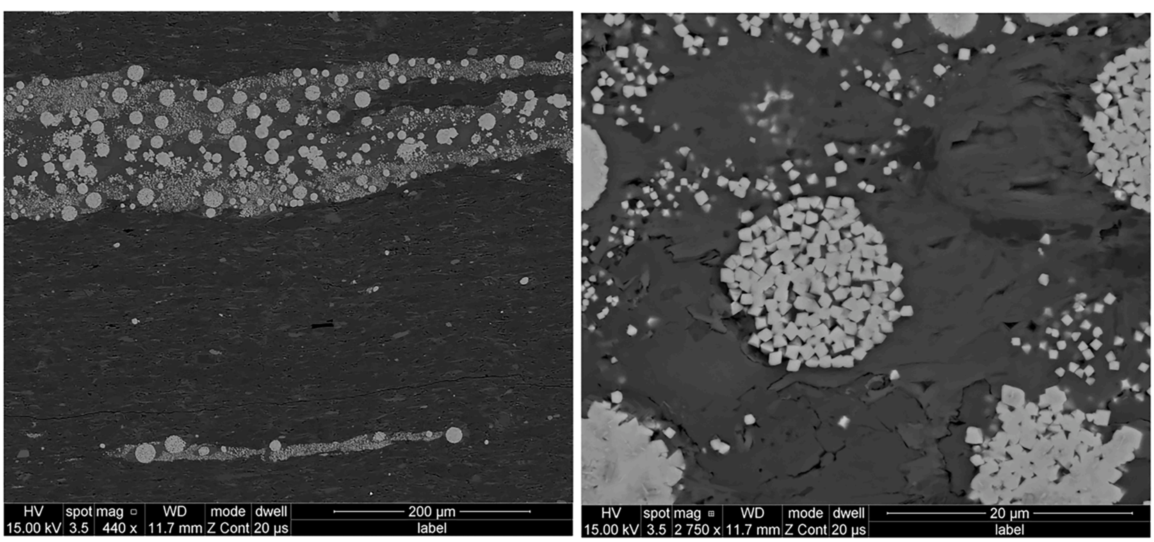

Fig. 9. (A) BSE image of the pyrite (bright spots, indicating relatively heavier elements) in the Chingshui geothermal pelite (relatively lighter elements). (B) Zooming in on these bright spots reveals cube and framboidal pyrite.

experiment was carried out without intentionally isolating the environment from oxygen. The newly formed secondary minerals after the water-rock reactions were clay minerals with a curled flake morphology. This result suggests conditions resembling surface oxidizing alteration, rather than an equilibrium between albite and illite in a reducing environment. The inability of the C_{Na}/C_K ratio to exhibit a linear relationship with temperature suggests that the Na/K geothermometer is not applicable in oxidizing environments.

3.5. Estimating the equilibrium time of fluid

It is widely believed that the Na/K geothermometer necessitates a longer period to attain equilibrium compared to other commonly used silica geothermometers (Fournier, 1989). Given the prevalence of quartz in the metapelitic geothermal field, feldspar and illite/muscovite make up only a small weight percentage of the metapelite. Additionally, the thermal fluids show reduced weakly acidic traits, with a pH value of approximately 6.39 at a depth of 803 m (Hsieh et al., 2021). Therefore, achieving sodium-potassium equilibrium in the metapelite area would necessitate a longer duration. We attempted to estimate the time required for equilibrium between albite, illite, and the hot fluid using the example of the Chingshui geothermal field. Residence times and rates of natural annual recharges were estimated through various methods. Fan et al. (2006) utilized tracer and interference tests to estimate a residence time of 15 years and a recharge rate of 1.3×10^7 m^3/year. Similarly, Cheng et al. (2010) analyzed naturally occurring tritium and carbon-14 in groundwater, estimating residence times between 11.3 and 15.2 years, with recharge rates ranging from 5.0×10^5

Table 4
Redox potential and pH of hot springs in metapelite.

Location	Type	Date	Longitude	latitude	T (°C)	pH (Field)	Eh (mv)	TDS (mg/L)	EC (μs/cm)	Salinity (psu)	Cl^- (mg/L)	SO_4^{2-} (mg/L)	CO_3^{2-} (mg/L)	HCO_3^- (mg/L)	SiO_2 (mg/L)	Na^+ (mg/L)	NH_4^+ (mg/L)	K^+ (mg/L)	Ca^{2+} (mg/L)	Mg^{2+} (mg/L)	Fe^{3+} (mg/L)	Mn^{2+} (mg/L)
Chingshui	boiling spring	2024.03.25	121°38′3.39″	24°36′46.83″	98.7	9.7	−492.5	2025	4049	2.14	9.04	28.8	462	1800	294	755	3.14	43.2	1.33	b.d.l.	b.d.l.	b.d.l.
Chingshui	Shallow well	2024.03.25	121°38′12.64″	24°36′37.54″	>35.7	5.8	−57.6	384	769	0.41	7.07	2.02	0	897	51.8	156	7.19	9.22	27.9	6.52	32.3	0.25
Chingshui	hot spring	2021.02.20	121°38′14.25″	24°36′48.82″	44.9	6.3	+73.9	532	1065	0.55	9.87	37.5	0	769	35.1	215	36.4	17.9	24.5	17.6	5.35	1.65
Chingshui	hot spring	2019.11.01	121°38′27.02″	24°36′35.47″	32.6	5.5	+137	273	545	0.29	2.27	130	0	317	36.0	1.62	1.84	1.06	62.6	25.9	b.d.l.	b.d.l.
Chingshui	hot spring	2018.09.30	121°38′1.85″	24°36′45.80″	58.3	5.8	+59.6	415	830	0.39	3.99	41.7	0	573	78.3	150	8.81	4.80	33.0	13.4	b.d.l.	b.d.l.
Chingshui	hot spring	2018.09.30	121°38′2.61″	24°36′47.65″	47.5	5.6	+70.9	269	537	0.26	4.33	43.8	0	525	44.2	100	6.86	5.26	15.0	8.49	b.d.l.	b.d.l.
Lushan	hot spring	2023.02.24	121°11′22.97″	24°1′8.07″	35.2	6.7	+17.2	501	1002	0.54	2.72	69.6	0	903	39.0	156	3.22	4.12	82.6	34.5	b.d.l.	3.58
Lushan	hot spring	2023.11.25	121°11′18.76″	24°1′15.19″	33.5	6.6	+105	427	853	0.46	2.28	70.8	0	683	25.7	104	2.41	3.84	73.3	17.8	0.23	4.15
Lushan	hot spring	2024.02.23	121°1′07.04″	24°1′20.26″	40.6	6.7	−7.7	944	1888	1.04	6.00	172	0	1720	0.90	488	6.83	8.14	128	42.6	b.d.l.	1.41

to 6.7×10^5 m^3/year.

Our sampling of geothermal fluid in 2017, approximately 24 years after the closure of the pilot geothermal power plant, demonstrated equilibrium among albite, illite, and the hot fluid. However, Huang et al. (2018) discovered that even after 60 days of experimentation, equilibrium among albite, illite, and the hot fluid had not been attained. This indicates that the time required for approaching equilibrium between albite, illite, and the hot fluid ranges from over 2 months to <15 years. Certainly, we cannot entirely dismiss the possibility that equilibrium may not be fully achieved in such a short time and that the system is merely "approaching equilibrium," which could explain the R^2 value of only 0.71.

3.6. *Investigation into the inconsistency between Na/K geothermometer and quartz geothermometer*

The hot fluids from both the Chingshui geothermal production wells (R1, R3, and R5) and the Tuchang-Jentse production wells (ZJ-14 and ZJ-15) exhibit discrepancies between the Na/K geothermometer and quartz geothermometer (Fig. 10). Specifically, all of these wells display quartz geothermometer temperatures notably lower than those indicated by the Na/K geothermometer (Table 2). Additionally, in the former, Cl^- concentrations are higher compared to other wells in Chingshui, while SO_4^{2-} concentrations are lower. Conversely, in the latter, Cl^- concentrations are much lower compared to other wells in Tuchang-Jentse, but SO_4^{2-} concentrations are significantly higher (Table 2).

In the case of Chingshui geothermal field, we hypothesize that nearby injection wells (located at distances of only 363 m, 337 m, and 500 m from R1, R3, and R5, respectively) may be contributing factors. The injected hot fluid, upon mixing with water from deeper wells, likely leads to higher Cl^- concentrations and lower SO_4^{2-} concentrations. Consequently, both the Na/K geothermometer and quartz geothermometer temperatures are notably higher than those measured at the wellheads (Table 2). Additionally, the process of flash, heat exchange, precipitation, and reinjection likely alters the Na/K equilibrium between the hot water and the albite and illite present in the metapelite.

In the case of ZJ-14 in the Tuchang-Jentse geothermal field, the lower Cl^- and higher SO_4^{2-} concentrations, coupled with quartz geothermometer temperatures being lower than the measured temperatures, while Na/K geothermometer temperatures are closer to the measured temperatures, suggest a possible infiltration of shallow groundwater causing dilution of the pear concentrate. The absence of a similar trend in the Lushan well suggests the possibility of faster or shallower water circulation, as indicated by the MT surveys. Low resistivity (indicating hot water) appears above an elevation of 500 m (Yueh-Iuan Ger, unpublished data), in contrast to Chingshui, where hot water can be traced rising along steep faults (Chang et al., 2014). However, some effects are difficult to explain with a single factor. For instance of ZJ-15, the decrease in Cl^- concentration and the increase in SO_4^{2-} concentration suggest the dilution effect of shallow groundwater infiltration. However, the temperatures indicated by the quartz geothermometer and Na/K geothermometer are higher than the actual measured temperatures. Additional data, such as δ^2H and $\delta^{18}O$ values, are required to fully explain these discrepancies.

4. Conclusion

The metapelitic geothermal fields in the Taiwan orogenic belt are uniquely characterized by "non-volcanic activity." These fields rely on collision-induced high geothermal gradients to heat deep circulating meteoric water, achieving Na-K equilibrium through water-rock reactions primarily involving albite and illite. The Na/K geothermometer can be used to estimate the reservoir temperature above 180 °C using the following equation:

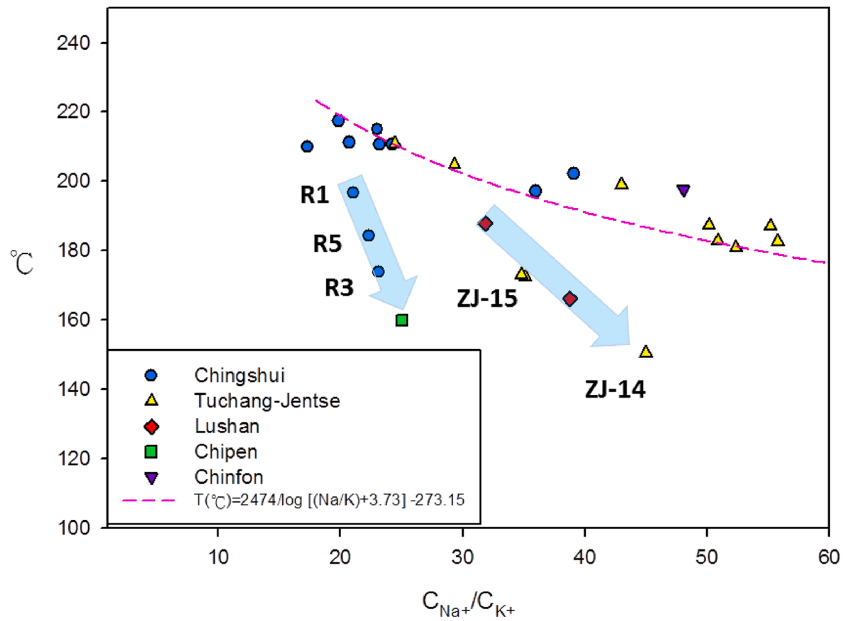

Fig. 10. After 2018, the R1, R3, R5 wells in the Chingshui geothermal field, as well as the ZJ-14 and ZJ-15 wells in Tuchang-Jentse, showed a decrease T_{SiO2} and an increase in C_{Na}/C_K. Interestingly, these trends align with the measurements from Chipen and Lushan.

$$T > 180^{\circ}C,\ T(^{\circ}C) = \frac{2474}{\log\left(\frac{Na}{K}\right) + 3.73} - 273.15$$

Water chemistry analysis and mineralogical identifications show that the redox environment plays a crucial role in maintaining the mineral equilibrium of N/K water-rock interactions in the metapelitic geothermal field. In the deep subsurface, where dissolved CO_2 has not yet escaped, the pH is weakly acidic (6.4, Hsieh et al., 2021). Despite this, under reducing conditions, albite and illite can still reach equilibrium. As hydrothermal fluids ascend from deeper to shallower levels, the escape of carbon dioxide causes the pH to rise to 8.0–9.6. If the fluids oxidize and dissolve the pyrite in the shallow subsurface, it leads to an increase in SO_4^{2-} concentrations, which can lower the pH to 5.6 or even lower. This acidification of the hydrothermal fluids leads to the formation of potassium-bearing clay minerals, such as alunite, kaolinite, Na-montmorillonite, or jarosite. Under these conditions, where multiple minerals with varying reactions and equilibria are involved, the Na/K geothermometer cannot accurately estimate the reservoir temperature in metapelite.

Considering the various constraints posed by factors such as temperature, redox conditions, and the duration of thermal water interaction with surrounding rocks, our stance remains firm that the silica geothermometer stands as the most reliable tool for assessing reservoir temperatures in Taiwanese metamorphic terrains. Especially in the future, if there are plans to undertake the development of Enhanced Geothermal Systems (EGS). While the Na/K geothermometer certainly has its utility, it should be viewed primarily as supplementary and utilized when favorable conditions permit. Given that the quartz geothermometer may be influenced by factors like evaporation, dilution, and mixing processes, incorporating the Na-K geothermometer provides additional support for evaluating reservoir temperatures, boiling phenomena, and the mixing dynamics of thermal fluids.

CRediT authorship contribution statement

Yi-Chia Lu: Writing – review & editing, Writing – original draft, Methodology, Investigation, Conceptualization. **Sheng-Rong Song:** Supervision, Investigation. **Ting-Jui Song:** Formal analysis, Data curation. **Chyi Wang:** Writing – review & editing, Supervision. **Andrew Tien-Shun Lin:** Validation, Supervision, Data curation. **Sachihiro Taguchi:** Writing – review & editing, Supervision.

Declaration of competing interest

The authors declare the following financial interests/personal relationships which may be considered as potential competing interests:|

Yi-Chia Lu reports financial support, administrative support, and article publishing charges were provided by Ministry of Science and Technology. Sheng-Rong Song reports a relationship with CPC Corporation Exploration and Production Business Division that includes: speaking and lecture fees and travel reimbursement.

Data availability

Data will be made available on request.

Acknowledgements

This work was supported by the Ministry of Science and Technology (MOST), Taiwan [MOST 103-3113-M-002-001, MOST 104-3113-M-002-001, MOST 105-3113-M-002-001, and NSTC 111-2116-M-008-022-MY3]. We want to express sincere appreciation to Fabulous Power Co. Limited for sampling the hot fluid in the Chingshui geothermal field.

To enhance the fluency and clarity of this manuscript, ChatGPT, an AI language model, has been utilized to assist in revising and refining the text. However, all original data, manuscript structure, and ideas presented in this paper are the work of the authors.

Supplementary materials

Supplementary material associated with this article can be found, in the online version, at doi:10.1016/j.geothermics.2024.103133.

References

Arnórsson, S., Gunnlaugsson, E., Svavarsson, H., 1983. The chemistry of geothermal waters in Iceland. III: chemical geothermometry in geothermal investigations. Geochim. Cosmochim. Acta 47, 567–577.

Asta, M.P., Gimeno, M.J., Auqué, L.F., Gómez, J., Acero, P., Lapuente, P., 2010. Secondary processes determining the pH of alkaline waters in crystalline rock systems. Chem. Geol. 276, 41–52. https://doi.org/10.1016/j.chemgeo.2010.05.019.

Byrne, T., Chan, Y.C., Rau, R.J., Lu, C.Y., Lee, Y.H., Wang, Y.J., 2011. The arc–continent collision in Taiwan. In: Brown, D., Ryan, P.D. (Eds.), Arc-Continent Collision. Springer Berlin Heidelberg, Berlin, Heidelberg, pp. 213–245.

Cacace, M., Blöcher, G., Watanabe, N., Moeck, I., Börsing, N., Kolditz, O., et al., 2013. Modelling of fractured carbonate reservoirs: outline of a novel technique via a case study from the Molasse Basin,southern Bavaria(Germany). Environ. Earth Sci. Epub 21, 18.

Can, I., 2002. A new improved Na/K geothermometer by artifcial neural networks. Geothermics 31 (6), 751–760.

Chan,Y.K., Lee, H.H., Yang, K.H., Wu, K.H., Lee, C.Y., 1986. Geologic map of the Jentse, Tuchang Geothermal Area, Ilan. Internal report of CPC Taiwan, 24 (Chinese content).

Chang, P.T., Chiao, C.H., 1979. Geology of the lushan geothermal area. Mining Mectall. 23 (2), 65–72.

Chang, P.Y., Lo, W., Song, S.R., Ho, K.R., Wu, C.S., Chen, C.S., Lai, Y.C., Chen, H.F., Lu, H.Y., 2014. Evaluating the Chingshui geothermal reservoir in northeast Taiwan with a 3D integrated geophysical visualization model. Geothermics 50, 91–100.

Chen, B.C., Perdana, T., Kuo, L.W., 2021. Fluid flow and fault-related subsurface fractures in slate and metasandstone formations: a case study of the Jentse Geothermal Area, Taiwan. Geothermics 89 (101986), 1–15.

Chen, B.C., Perdana, T., Kuo, L.W., 2023. Geophysical characteristics of a fault system in the northern Central Range of Taiwan and its applications for geothermal energy exploration. Geothermal Energy 11 (1), 22.

Chen, C.H., 1975. Thermal waters in Taiwan, a preliminary study. In: Proc. Grenoble Symp., Aug. 1975, Int. Assoc. Hydrol. Sci., Publ. No. 119, pp. 79–88.

Chen, C.H., 1982. Analysis of topographic effect on ascending thermal water in the Central Range of Taiwan. Proc. Natl. Sci. Counc., Part A 6, 241–249.

Chen, C.H., 1985. Water-Rock Interaction Chemical characteristics of thermal waters in the Central Range of Taiwan. R.O.C. Chem. Geol. 49, 303–317.

Chen, C.T., Chan, Y.C., Beyssac, O., Lu, C.Y., Chen, Y.G., Malavieille, J., Kidder, S.B., Sun, H.C., 2019. Thermal history of the northern taiwanese slate belt and implications for wedge growth during the neogene arc-continent collision. Tectonics 38 (9), 3335–3350.

Chen, P.C., 2011. Distribution of Hot Springs in Taiwan and Geological Significance of fluid characteristics. 2011 research and development special report. Central Geological Survey. MOEA, Taiwan, 335 p.p. (Chinese content.

Chen, W.S., Wang, Y., 1988b. In: The Plio-Pleistocene Basin Development In The Coastal Range Of Taiwan. Symposium on the Arc-Continent Collision and Orogenic Sedimentation in Eastern Taiwan and Ancient Analogs. Handbook, Taiwan, ROC, pp. 21–22 (Chinese content).

Chen, W.S., Wang, Y., 1996. Geology of the eastern coastal mountains of Taiwan. Central Geological Survey, Ministry of Economic Affairs, 101 (Chinese content).

Chen, W.S., 2016. An Introduction to the Geology of Taiwan explatory Text of the Geologic Map of Taiwan (1/400000). Geological Society Located in Taipei (Chinese content).

Cheng, W., Kuo, T., Su, C., Chen, C., Fan, K., Liang, H., Han, Y., 2010. Evaluation of natural recharge of Chingshui geothermal reservoir using tritium as a tracer. Radiat. Meas. 45, 110–117. https://doi.org/10.1016/j.radmeas.2009.08.002.

Ching, K.E., Hsieh, M.L., Johnson, K.M., Chen, K.H., Rau, R.J., Yang, M., 2011. Modern vertical deformation rates and mountain building in Taiwan from precise leveling and continuous GPS observations, 2000–2008. Jour. Geophy. Res. 116 https://doi.org/10.1029/2011JB008242.

Dadson, S.J., Hovius, N., Chen, H., Dade, W.B., Hsieh, M.L., Willett, S.D., Hu, J.C., Horng, M.J., Chen, M.C., Stark, C.P., Lague, D., Lin, J.C., 2003. Links between erosion, runoff variability and seismicity in the Taiwan orogen. Nature 426, 648–651.

Deon, F., Moeck, I., Jaya, M., Wiegand, B., Scheytt, T., Putriatni, D.J., 2012. Preliminary assessment of the geothermal system in the Tiris volcanic area, East Java, Indonesia. In: Proceedings of the 74th EAGE conference and exhibition. Copenhagen, Denmark. EarthDoc EAGE Publications.

Diamond, L.W., Wanner, C., Waber, H.N., 2018. Penetration depth of meteoric water in orogenic geothermal systems. Geology; 46 (12), 1063–1066. https://doi.org/10.1130/G45394.1.

Diaz-Gonzalez, L., Santoyo, E., Reyes-Reyes, J., 2008. Tres nuevos geotermómetros mejorados de Na/K usando herramientas computacionales y geoquimiométricas: aplicación a la predicción de temperaturas de sistemas geotérmicos. Revista Mexicana de Ciencias Geológicas; 25 (3), 465–482.

Ellis, A.J., Wilson, S.H., 1960. The geochemistry of alkali metal ions in the Wairakei hydrothermal system. N. Z. J. Geol. Geophys. 3, 593–617.

Ellis, A.J., Mahon, W.A.J., 1964. Natural hydrothermal systems and experimental hotwater rock interactions. Geochim. Cosmochim. Acta 28, 1323–1357.

Fan, K.C., Kuo, M.C.T., Chen, C.J., 2006. Evaluation of natural recharge of chingshui geothermal reservoir in Taiwan. In: Thirty-First Workshop on Geothermal Reservoir Engineering Stanford University. Stanford, California.

Faulds, J.E., Bouchot, V., Moeck, I., Oguz, K., 2009. Structural controls of geothermal systems in western Turkey: a preliminary report. Geotherm. Resou. Counc. Trans. 33, 375–383.

Fournier, R.O., 1977. Chemical geothermometers and mixing models for geothermal systems. Geothermics 5 (1–4), 41–50.

Fournier, R.O., 1979. A revised equation for the Na/K geothermometer. Geotherm. Res. Council Transac. 3, 221–224.

Fournier, R.O., 1989. Lectures on Geochemical Interpretation of Hydrothermal Waters. UNU Geothermal Training Programme.

Fournier, R.O., Rowe, J.J., 1966. Estimation of underground temperatures from the silica content of water from hot springs and wet-steam wells. Am. J. Sci. 264, 685–697.

Fournier, R.O., Truesdell, A.H., 1974. Geochemical indicators of subsurface temperature: part ii estimation of temperature and fraction of hot water mixed with cold water 2. U.S. Geological Survey 263–270.

Giggenbach, W.F., 1988. Geothermal solution equilibria. Derivation of Na-K-Mg-Ca geoindicators. Geochim. Cosmochim. Acta 52, 2749–2765.

Grasby, S.E., Hutcheon, I., 2001. Controls on the distribution of thermal springs in the southern Canadian Cordillera. Can. J. Earth Sci. 38, 427–440. https://doi.org/10.1139/e00-091.

Ho, C.S., 1986. A synthesis of geologic evolution of Taiwan. Tectonophysics 125, 1–16.

Ho, G.R., Chang, P.Y., Lo, W., Liu, C.M., Song, S.R., 2014. New evidence of regional geological structures inferred from reprocessing and resistivity data interpretation in the Chingshui-Sanshing-Hanchi area of southwestern Ilan County, NE Taiwan. Terr. Atmos. Ocean. Sci. 25 (4), 491–504.

Hsiao, P.T., Tseng, C.S., Wey, S.K., 1980. Geology and geothermal potential, Lushan. Petrol. Geol. Taiwan 17, 107–123 (Chinese content).

Hsiao, P.T., Chiang, S.C., 1979. Geology and geothermal system of the Chingshui-Tuchang geothermal area, Ilan, Taiwan. Petrol. Geol. Taiwan 16, 205–213 (Chinese content).

Hsieh, P.S., Lin, C.K., Chang, Y.T., Lu, H.Y., Yang, T.S., 2021. The GTFSampler: a new downhole equipment for geothermal fluid sampling and its testing results in the Chingshiu geothermal field, Ilan, Taiwan. Geothermics 94, 102077. https://doi.org/10.1016/j.geothermics.2021.102077.

Hsu, W.H., Byrne, T.B., Ouimet, W., Lee, Y.H., Chen, Y.G., Soest, M.v., Hodges, K., 2016. Pleistocene onset of rapid, punctuated exhumation in the eastern Central Range of the Taiwan orogenic belt. Geology 44, 719–722.

Huang, Y.H., Liu, H.L., Song, S.R., Chen, H.F., 2018. An ideal geothermometer in slate formation: a case from the Chingshui geothermal field, Taiwan. Geothermics 74, 319–326.

ITRI, 1994. Compilation of Geothermal Exploration Data in Taiwan. Energy Research and Development Fund Research Report (No.: 06-3-83-0252-2). Energy Committee of the Ministry of Economic Affairs. 538. (Chinese content).

ITRI, 2010. Development of Sustainable Technologies for Traditional and Deep Geothermal Energy (1/4). (Chinese content).

ITRI, 2012. Development of Sustainable Technologies for Traditional and Deep Geothermal Energy (3/4) (Chinese content).

Jhan, Y.K., Lee, H.H., Yang, K.H., Wu, K.H., Lee, C.Y., 1986. Geological Report of the Jentse and Tuchang Geothermal Area, I-Lan. Reoprt of Geothermal Division, Taiwan Oil Exploration Office, Taiwan, pp. 1–22 (Chinese content).

Lee, P.Y., 1977. Rate of the Early Pleistocene uplift in Taiwan. Mere. Geol. Soc. China 2, 71–76.

Lin, C.C., 1957. Geomorphology of Taiwan. Taiwan Provincial Literature 1 (1), 1–424.

Lin, C.W., Lin, W.H., 1995. Explanatory Text of the Geologic Map of Taiwan Sanshin. Sheet 15. Cent. Geol. Surv. MOEA, Taiwan. (Chinese content).

Liu, K.K., Yui, T.F., Shieh, Y.N., Chiang, S.C., LH, C., Ho, J.Y., 1990. Hydrogen and oxygen isotope compositions of meteoric and thermal waters from the Chingshui geothermal area, northeastern Taiwan. Proc. Geol. Soc. China 33, 143–165.

Liu, T.K., 1982. Tectonic implication of fission track ages from the Central Range, Taiwan. Proc. Geol. Soc. China 25, 22–37.

Liu, T.K., Hsieh, S., Chen, Y.G., Chen, W.S., 2001. Thermo-kinematic evolution of the Taiwan oblique-collision mountain belt as revealed by zircon fission track dating. Earth Planet. Sci. Lett. 186, 45–56.

Lo, F.L., Chen, H.F., Fang, J.N., 2017. Discussion of suitable chemical weathering proxies in sediments by comparing the dissolution rates of minerals in different rocks. J. Geol. 125 (1), 83–99.

Lu, Y.C., Song, S.R., Wang, P.L., Wu, C.C., Mii, H.S., MacDonald, J., Shen, C.C., John, C.M., 2017. Magmatic-like fluid source of the Chingshui geothermal field, NE Taiwan evidenced by carbonate clumped-isotope paleothermometry. J. Asian Earth Sci. 149, 124–133.

Lu, Y.C., Song, S.R., Taguchi, S., Wang, P.L., Yeh, E.C., Lin, Y.J., MacDonald, J., John, C. M., 2018. Evolution of hot fluids in the Chingshui geothermal field inferred from crystal morphology and geochemical vein data. Geothermics 74, 305–318.

Lu, Y.C., Song, S.R., Lin, P.H., Taguchi, S., Wang, C., Lai, Y.M., Lee, H.F., 2020. Thermal fluid changes after operating a geothermal system: a case study of the Chingshui Geothermal Field, Taiwan. Geothermics 87, 101878.

Lu, Y.C., Song, S.R., Liu, L.W., Peng, T.R., Chen, B.C., Tu, K.C., Lin, L.H., Wang, P.L., 2023. Applicability of carbonate clumped isotope thermometry in the Tuchang-Jentse geothermal field. Geothermics 112, 102728.

M.R.S.O., 1975. Exploration Of Geothermal Resources In Taiwan - Report No.1 (From January 1973 to December 1974). Miming Research and Service Organization industrial technology research institute Report, 147. (In Chinese).

Moeck, I., 2014. Catalog of geothermal play types based on geologic controls. Renew. Sustain. Energy Rev. 37, 867–882.

Nieva, D., Nieva, R., 1987. Developments in geothermal energy in Mexico—Part twelve. A cationic geothermometer for prospecting of geothermal resources. Heat Recov. Syst. CHP 7 (3), 243–258.

Nisbet, E.G., Fowler, C.M.R., 1982. The thermal background to metamorphism, 1. Simple onedimensional conductive models. Geosci. Can. 9, 161–164.

Nukman, M, Moeck, I., 2013. Structural controls of a geothermal system in the Tarutung Basin, north central Sumatra. J Asian Earth Sci 74, 86–96.

Reyes, A.G., Christenson, B.W., Faure, K., 2010. Sources of solutes and heat in low-enthalpy mineral waters and their relation to tectonic setting, New Zealand. J. Volcanol. Geotherm. Res. 192, 117–141. https://doi.org/10.1016/j.jvolgeores.2010 .02.015.

Reyna-Avilez, A., Gómez-Arias, E., Valencia-Cabrera, D., Tello-Hinojosa, E., González-Fernández, A., Pérez-Flores, M.A., 2023. Fluid-rock mineral equilibrium and new improved Na/K geothermometers: the case of the Cerro Prieto geothermal field (CP-I), Mexico. Geothermics 115, 102822.

Seno, T., Maruyama, S., 1984. Paleogeographic reconstructionand origin of the Philippine sea. Tectonophysics 102, 53–84.

Shen, T.T., Liu, T.K., Huang, S.Y., Hsieh, P.S., Wu, C.Y., 2020. Post-collisional exhumation and geotherm pattern in northern Tananao Complex, northeastern Taiwan. Terr. Atmospheric Ocean. Sci. 31, 369–381.

Shi, Z., Liao, F., Wang, G., Xu, Q., Mu, W., Sun, X., 2017. Hydrogeochemical characteristics and evolution of hot springs in Eastern Tibetan Plateau geothermal belt, Western China: insight from multivariate statistical analysis. Geofluids 2017.

Sonney, R., Vuataz, F.-D., 2009. Numerical modelling of Alpine deep flow systems: a management and prediction tool for an exploited geothermal reservoir (Lavey-les-Bains, Switzerland). Hydrogeol. J. 17, 601–616. https://doi.org/10.1007/s10040-008-0394-y.

Stober, I., Zhong, J., Zhang, L., Bucher, K., 2016. Deep hydrothermal fluid-rock interaction: the thermal springs of Da Qaidam, China. Geofluids 16, 711–728. https://doi.org/10.1111/gfl.12190.

Suppe, J., 1981. Mechanics of Mountain Building and Metamorphism in Taiwan. Memoir of the Geological Society of China, No. 4, 67-89.Fournier, R.O., Potter, R.W.: revised and expanded silica (quartz) geothermometer. Geotherm. Res. Council Bull. 11, 3–12.

Teng, L.S., 1987. Stratigraphic records of the late Cenozoic Penglai orogeny of Taiwan. Acta Gwl. Taiwan. 25, 205–224.

Teng, L.S., 1990. Geotectonic evolution of late Cenozoic arc-continent collision in Taiwan. Tecionophysics 183, 57–76.

Tsai, Y.B., Liaw, Z.S., Lee, T.Q., Lin, M.T., Yeh, Z.H., 1981. Seismological evidence of an active plate boundary in the Taiwan area. Mem. Geol. Sot. China 4, 143–154.

Tseng, C.S., 1978. Geology and Geothermal Occurrence of the Chingshui and Tuchang Districts, Ilan. Petrol. Geol. Taiwan 15, 11–23.

Tonani, F., 1980. Some Remarks on the Application of Geochemical Techniques in geothermal exploration. In: Strub, AS, Ungemach, P (Eds.), Advances in European geothermal research. Proceedings of the second international seminar on the results of EC geothermal energy research held in Strasbourg, 4–6 March 1980, Strasbourg.

Tong, L.T., Ouyang, S., Guo, T.R., Lee, C.R., Hu, K.H., Lee, C.L., Wang, C.J., 2008. Insight into the geothermal structure in Chingshui, Ilan, Taiwan. Terr. Atmos. Ocean. Sci. 19, 413–424.

Valencia-Cabrera, D., Gómez-Arias, E., Tello-Hinojosa, E., Reyna-Avilés, A., 2022. Fluid-rock mineral equilibrium and new improved Na/K geothermometer from Las Tres Vírgenes geothermal field, Mexico. In: Armstrong-Altrin, J.S., Pandarinath, K., Kumar-Verma, S. (Eds.), Geochemical Treasures and Petrogenetic processes. Editorial Springer Nature Singapore Pte Ltd, pp. 399–430 (ISBN 978-981-19-4781-0; ISBN electerónico 978-981-19-4782-7).

White, D.E., 1970. Geochemistry applied to the discovery, evaluation, and exploitation of geothermal energy resources. In: Proceedings of the United Nations Symposium on the Development and Utilization of Geothermal Resources. IIRG, CNR, Pisa, Italy, pp. 58–80.

Yu, S.B., Hsu, Y.J., Bacolcol, T., Yang, C.C., Tsai, Y.C., Solidum, R., 2013. Present-day crustal deformation along the Philippine Fault in Luzon, Philippines. J. Asian Earth Sci. 65, 64–74. https://doi.org/10.1016/j.jseaes.2010.12.007.

Yu, S.B., Chen, H.Y., 1994. Global Positioning System measurements of crystal deformation in the Taiwan arc-continent collision zone. Terr. Atom. Ocean. 5, 477–498.

Yui, T.F., Liu, K.K., Shieh, Y.N., 1993. Stable isotope systematics of pelite/slate from a deep well in the Chingshui geothermal field, Taiwan. Chem. Geol. 103, 181–191. https://doi.org/10.1016/0009-2541(93)90300-8.

Verma, S.P., Santoyo, E., 1997. New improved equations for Na/K, Na/Li and SiO_2 geothermometers by outlier detection and rejection. J. Volcanol. Geotherm. Res. 79 (1–2), 9–23.